Assessment of the RDGFLO3D for a Delta Wing at Low Reynolds Number (C2.2) and DNS of the Taylor-Green Vortex (C3.3)

Xiaodong Liu, Yidong Xia, and Hong Luo
Department of Mechanical and Aerospace Engineering
North Carolina State University
Raleigh, NC 27695, USA
Email: xliu29@ncsu.edu, hong_luo@ncsu.edu

1. Code Description

Numerical experiments for test cases C3.3 and C2.2 are conducted in this work using our RDGFLO3D (Reconstructed Discontinuous Galerkin FLow) code. The RDGFLO3D solves the compressible Navier-Stokes equations using a reconstructed discontinuous Galerkin (rDG) formulation on hybrid grids, which can contain one or combination of the four most common element types: tetrahedra, prisms, pyramids, and hexahedra. Our rDG method is based on a Hierarchical WENO reconstruction, termed HWENO(P1P2), which is designed not only to enhance the accuracy of the discontinuous Galerkin method but also to ensure the nonlinear stability of the rDG method[1,2]. In the HWENO(P1P2) method, a quadratic polynomial solution (P2) is first reconstructed using a WENO reconstruction from the underlying linear polynomial (P1) discontinuous Galerkin solution to ensure the linear stability of the rDG method and to improve the efficiency of the underlying DG method. The first derivatives of the quadratic polynomial solution are then reconstructed using a WENO reconstruction in order to eliminate spurious oscillations in the vicinity of strong discontinuities and thus ensure the nonlinear stability of the rDG method. Both the explicit three-stage third-order TVD Runge-Kutta scheme and implicit third-order Runge-Kutta or Rosenbrock schemes have been developed to advance solution in time for the unsteady flow problems[3,4]. A *p*-multigrid method has been developed to accelerate steady state solutions[5,6]. The parallelization of the RDGFLO3D code is achieved using a Message-Passing-Interface (MPI) programming paradigm based on the domain decomposition by METIS. The RDGFLO code can also be accelerated on GPUs using OpenACC. The RDGFLO3D code has been used to compute a variety of both steady-state and time-accurate flow problems on arbitrary grids. The numerical experiments indicate that the RDGFLO3D is able to provide sharp resolution of discontinuities essentially without any spurious oscillations, and achieve the designed third-order of accuracy for smooth flows in both space and time.

2. Case Description

The RDGFLO3D code has been used to compute two test cases in the workshop: C3.3 and C2.2. The first test case is the Taylor-Green vortex flow problem at a Reynolds number of 1,600 and a Mach number of 0.1. This test case is chosen to assess the DNS ability of the RDGFLO3D code. The initial condition for the Taylor-Green vortex is an

analytical function provided by the workshop. The numerical experiments are conducted using a second-order DG method and a 3rd order rDG method on different grid sizes to demonstrate the accuracy and performance of the RDGFLO3D code. All the quantities requested by the workshop are obtained and compared with the reference data. The second test case involves a laminar flow past a Delta Wing at a Reynolds number of 4,000 and at a Mach number of 0.3. This test case is chosen to test if the RDGFLO3D is able to effectively resolve the flow features in complex conditions. The flow is initialized from the uniform free stream condition. The numerical experiments are performed using a second-order DG method and a 3rd order rDG method to demonstrate the performance of the RDGFLO3D code. The density residual is used as the convergence indicator. Runs were performed on the ARC at the NC State University. All machines are 2-way SMPs with AMD Opteron 6128 (Magny Core) processors with 8 cores per socket (16 cores per node).

3. Meshes

Three hexahedral meshes, with 40x40x40, 81x81x81 and 161x161x161 cells, are used in the Taylor-Green vortex problem.

For Delta wing case, a sequence of 3 unstructured meshes, containing 15813, 95860 and 674260 tetrahedral elements, are used for the accuracy and efficiency study.

4. Results

The mesh and order refinement studies are all performed on multiple processors and work units are obtained using the formula shown below,

$$\text{Work units} = \frac{\text{Wall time x Number of cores}}{\text{TauBench time}}$$

where the average TauBench CPU time is 35.6 seconds.

4.1 3D Taylor-Green vortex flow

The change in the integrated kinetic energy E_k over time is shown for all three grid levels in figure 1. With grid resolution, the prediction of the integrated kinetic energy improves.

Figure 2-4 shows the evolution of the energy dissipation rate in several forms. The evolution of kinetic energy dissipation rate, $\epsilon = -dE_k/dt$, is given in figure 2. Here, the accuracy improves with grid resolution and the 161^3 grid is in excellent agreement with the reference solution. The evolution of enstrophy $\mathcal{E}$, is given in figure 3. For incompressible flow, $\mathcal{E} = \frac{1}{2}\frac{\rho 0}{\mu}\epsilon$, and one may expect the prediction of $\mathcal{E}$ and ϵ be similar. However as the figure shows, the enstrophy is more difficult to resolve numerically. The peak enstrophy is severely underpredicted on the coarsest grid. The prediction improves with grid resolution and the enstrophy on the 161^3 grid approaches the correct levels well. The primary contribution of the energy dissipation rate, ϵ_1, can be computed from the deviatoric portion of the strain rate tensor (figure 4). This prediction of this quantity is very similar to the prediction of the enstrophy evolution. The other contribution to the energy dissipation rate, ϵ_3, is from the product of pressure and

dilatation. For incompressible flow this term should be very small. With grid resolution, the prediction of ϵ_3 improves.

For this case, the Q criterion at t=8.0 is shown in figure 6, computed based on the rDGP1P2 scheme on the finest mesh. The resolution of the calculated turbulent structures is very similar to the illustration from other's reference [7]. On the 161^3 grid, the contour of the vorticity norm on the constant x-plane, $x = -\pi L$, at time t = 8 is shown in figure 7.

The time-stepping is done using a fourth order explicit Runge-Kutta with a fixed time step.

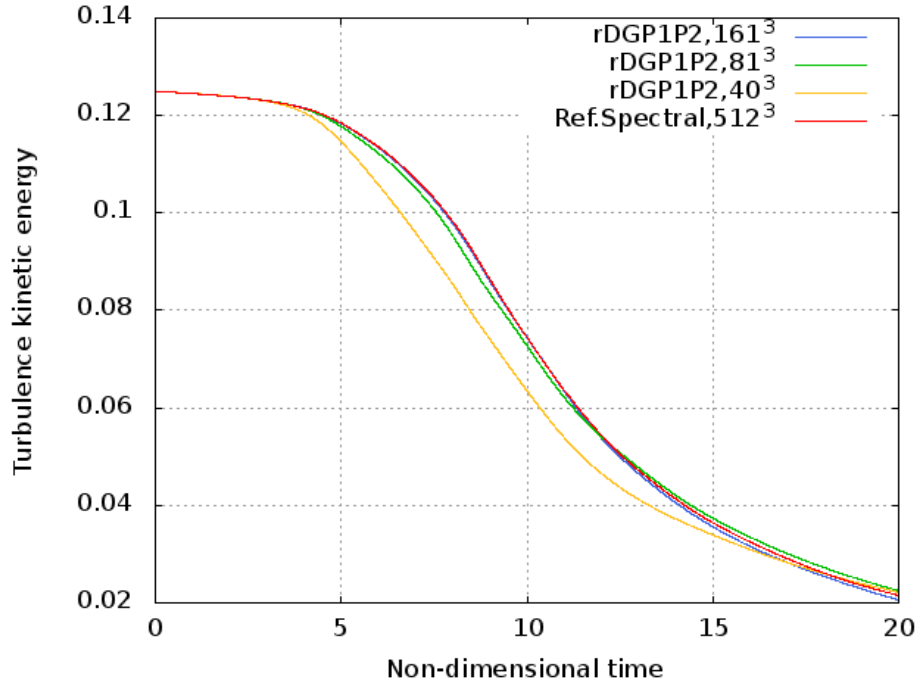

Fig. 1 Evolution of the dimensionless kinetic energy as a function of the dimensionless time.

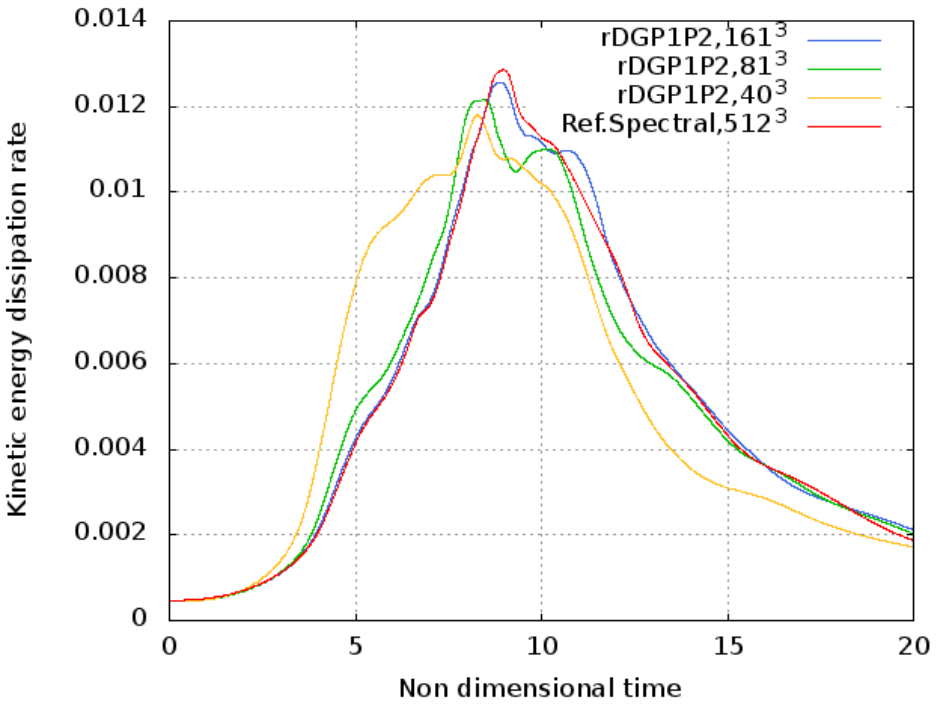

Fig. 2 Evolution of the dimensionless kinetic energy dissipation rate as a function of the dimensionless time.

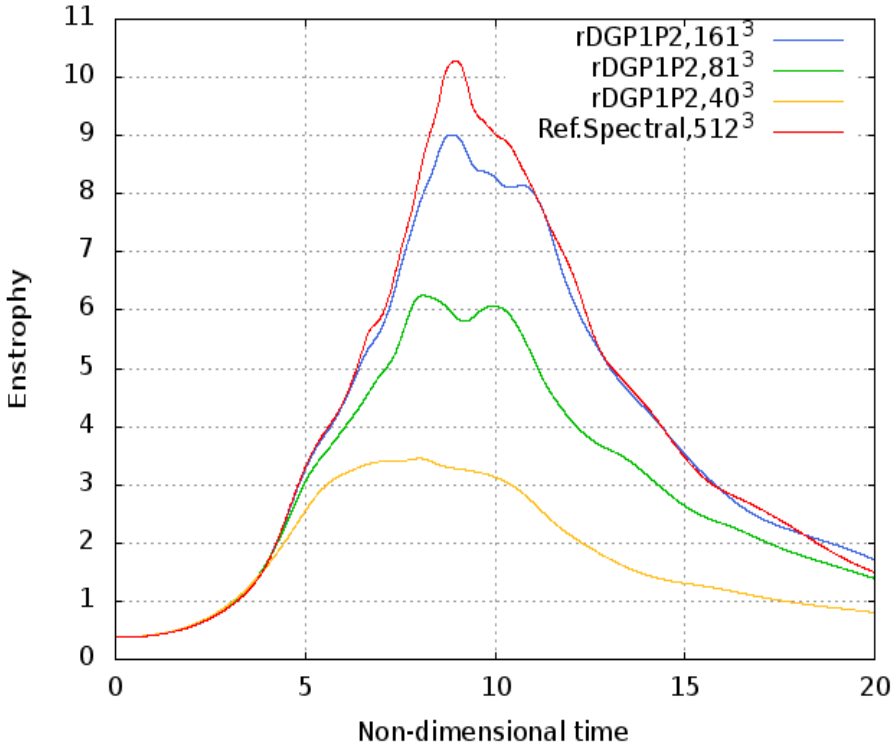

Fig. 3 Evolution of the dimensionless enstrophy as a function of the dimensionless time.

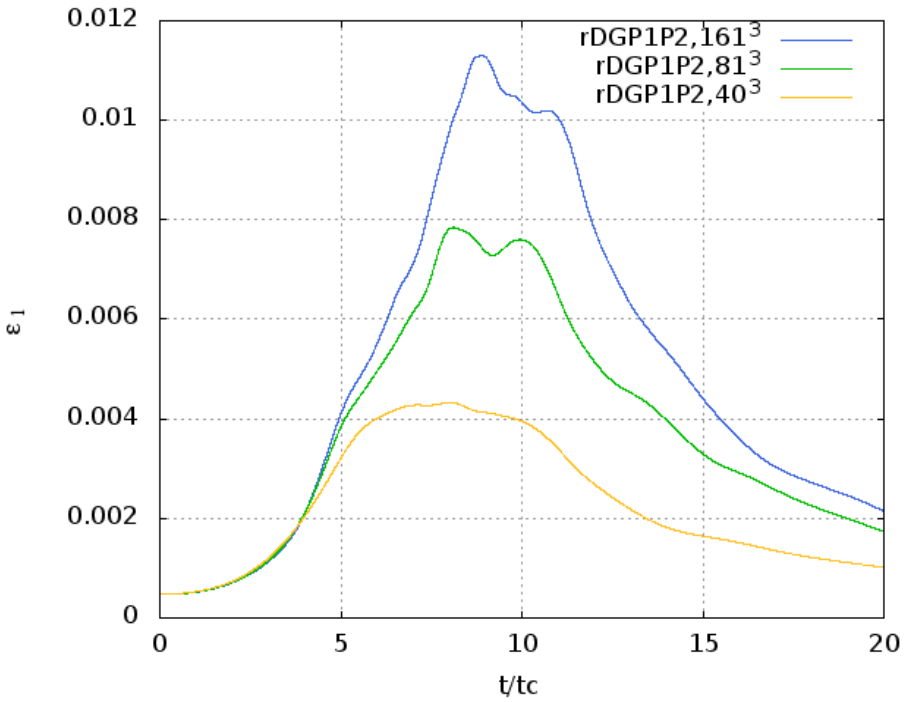

Fig. 4 Evolution of the dimensionless ϵ_1 as a function of the dimensionless time.

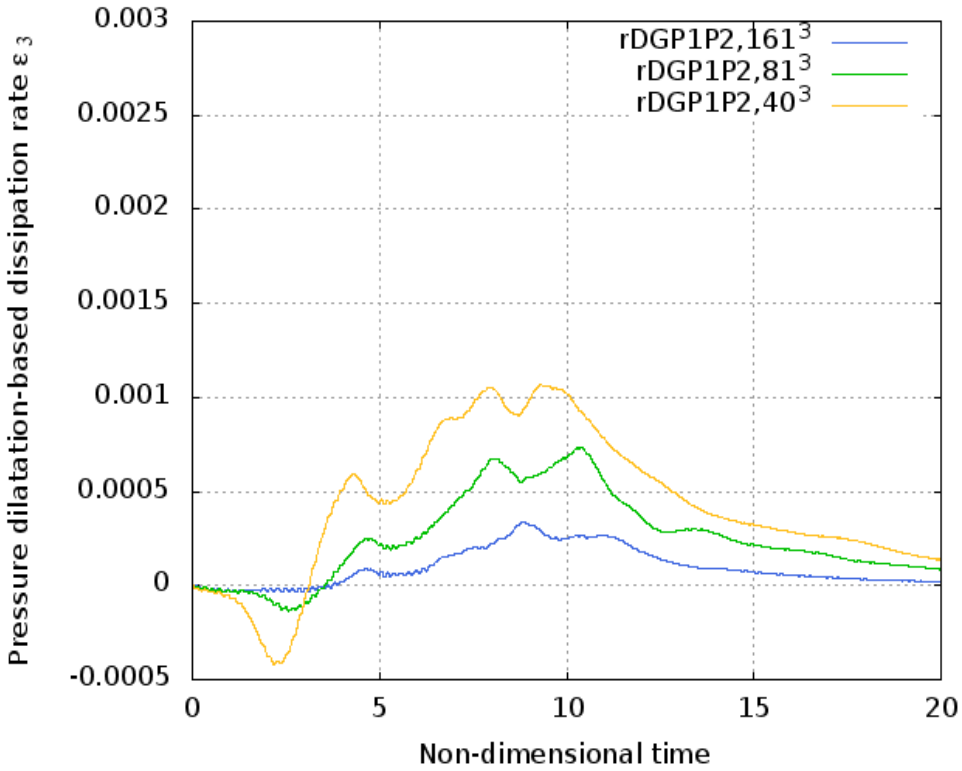

Fig. 5 Evolution of the dimensionless ϵ_3 as a function of the dimensionless time.

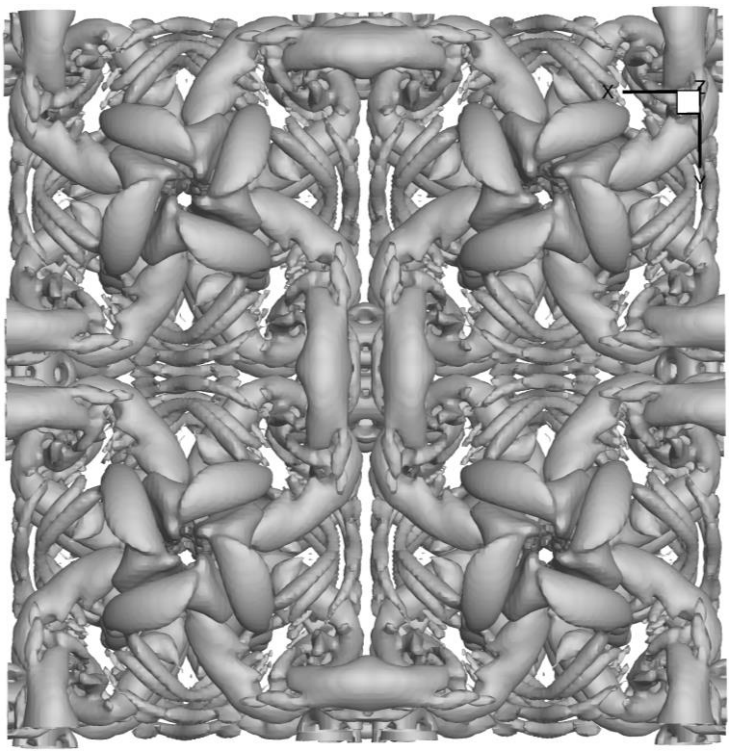

Fig.6 TGV solution on the finest mesh using rDGP1P2 scheme, showing iso-surfaces of Q criterion at time t=8.0 tc.

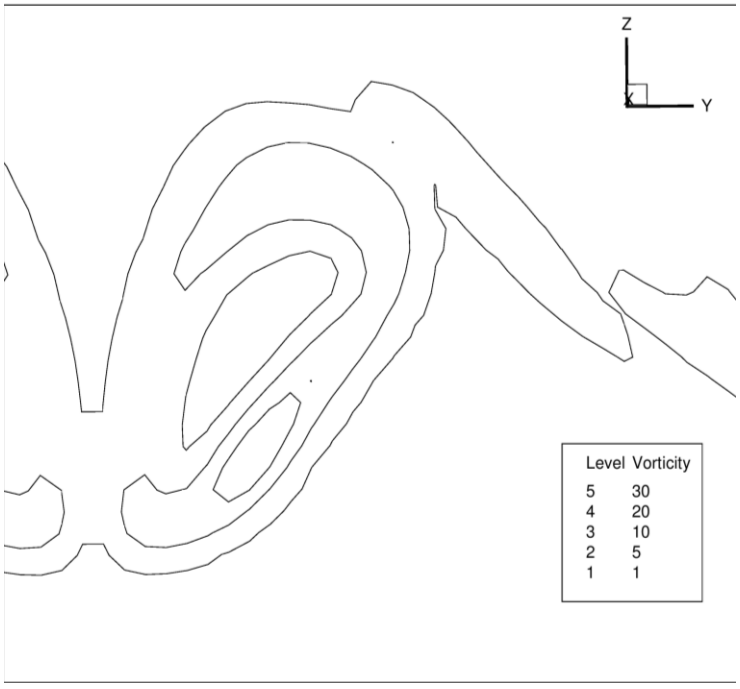

Fig.7 The contour of the dimensionless vorticity norm, at x = $-\pi$L and t = 8.0.

The simulation details and work units for such case are given in Table 1.

Table 1.The simulation details and work units of the DNS of Taylor-Green vortex.

Grid(Hex)	DOF	Time step	#of cores(# of processes)	Work units
40x40x40	256,000	4.00e-04	16(32)	1332
81x81x81	2,125,764	2.00e-04	16(32)	16202
161x161x161	16,693,124	8.00e-05	16(32)	261483

4.2 Laminar flow past a Delta Wing

In this code, no-slip and adiabatic wall boundary condition is prescribed on the wing surface. Tables 2 lists the number of degrees of freedom (nDoFs) per equation in the rDG solvers. All the cases were run on 32 processors with 16 cores.

Table 2. Number of degrees of freedom per equation in the DGP1 and rDGP1P2 schemes.

nDOFs	Mesh 0	Mesh 1	Mesh 2
DGP1	63,252	383,440	2,697,040
rDGP1P2	63,252	383,440	2,697,040

Viscous drag and lift coefficients are computed using the second-order DGP1 method and the third-order rDGP1P2 method as the steady state solution is achieved. The steady state is achieved while the solution vector itself stops changing.

Figure 8 shows lift (a) and drag (b) error convergence as a function of length scale (h=1/(nDoFs)^(1/3)) for the DG discretizations.

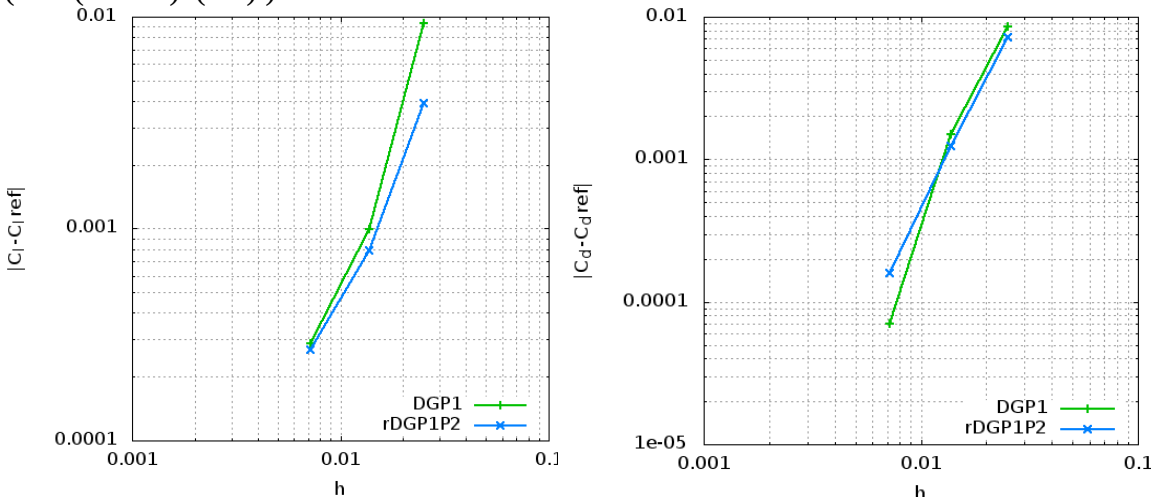

(a) C_l error vs. length scale **(b) C_d error vs. length scale**

Fig.8. Convergence of lift and drag error as a function of length scale for the DGP1 and rDGP1P2 methods in the laminar delta wing case (M=0.3, Re=4000, α=12.5°).

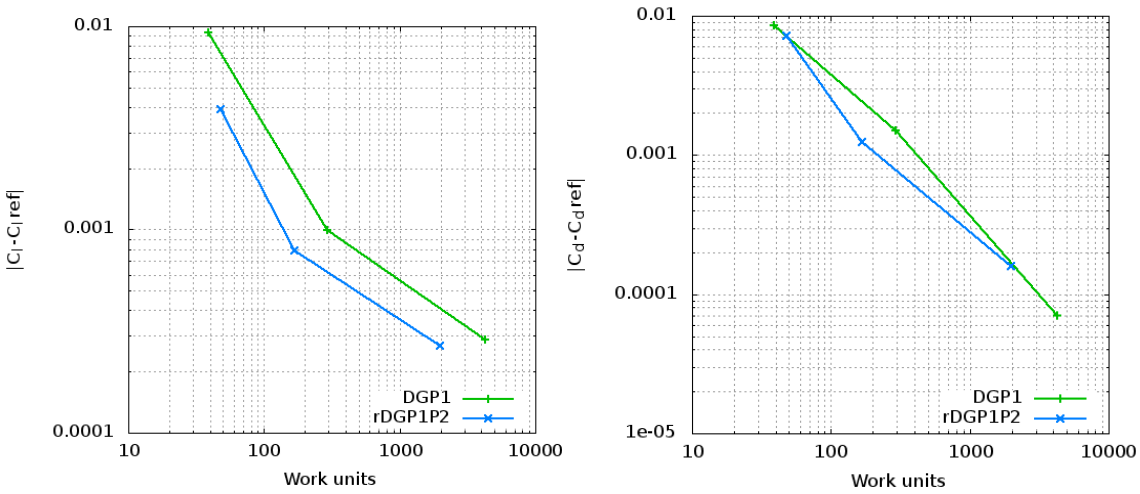

(a) C_l error vs. work units **(b) C_d error vs. work units**

Fig.9. Convergence of lift and drag error as a function of work units for the DGP1 and rDGP1P2 methods in the laminar delta wing case (M=0.3, Re=4000, α=12.5°).

Figure 9 displays a comparison of the force coefficients error convergence in terms of work units. It can be observed that the computational cost decreases with increasing discretization order from DGP1 to rDGP1P2.

Table 3 lists the lift and drag coefficients computed using DGP1 and rDGP1P2 methods on the 3 sets of meshes, where some non-monotonic convergence is shown using such schemes. This behavior may be caused by different wall boundary conditions implemented.

Table 3. Force coefficients computed by DGP1 and rDGP1P2 methods in the laminar delta wing case.

Schemes	Force coefficients	Mesh 0	Mesh 1	Mesh2
DGP1	Cl	0.33770726016	0.34601133389	0.34671154537
	Cd	0.17433304061	0.16729845718	0.16573001860
rDGP1P2	Cl	0.34307235112	0.34778998428	0.34726945097
	Cd	0.17295147182	0.16703650669	0.16595970175

References

1. Luo, H., Xia Y., Spiegel, S., Nourgaliev, R., Jiang, Z., A Reconstructed Discontinuous Galerkin Method Based on a Hierarchical WENO Reconstruction for Compressible Flows on Tetrahedral Grids, **Journal of Computational Physics**, Vol. 236, pp. 477-492, 2013
2. Luo, H., Xia Y., Li. S., Nourgaliev, R., and Cai, C., A Hermite WENO Reconstruction-Based Discontinuous Galerkin Method for the Euler Equations on Tetrahedral Grids, **Journal of Computational Physics**, Vol. 231, pp. 5489-5503, 2012.

3. Xia, Y., Luo, H., and Nourgaliev, R., An implicit Hermite WENO reconstruction-based discontinuous Galerkin method on tetrahedral grids, **Computers & Fluids**, 2014, http://dx.doi.org/10.1016/j.compfluid.2014.02.027
4. Xia, Y., Luo, H., Frisbey, M., and Nourgaliev, R., A Set of Parallel, Implicit Methods for a Reconstructed Discontinuous Galerkin Method for the Compressible Flows on 3D Arbitrary Grids, **Computers & Fluids**, 2014, http://dx.doi.org/10.10.16/j.compfluid.2014.01.023
5. Luo, H., Baum, J. D., and Löhner, R., Fast, *p*-Multigrid Discontinuous Galerkin Method for Compressible Flows at All Speeds, **AIAA Journal**, Vol. 46, No. 3, pp. 635-652, March 2008.
6. Luo, H., Baum, J. D., and Löhner, R., A *p*-Multigrid Discontinuous Galerkin Method for the Euler Equations on Unstructured Grids, **Journal of Computational Physics**, Vol. 211, No. 1, pp. 767-783, 2006.
7. Bull, J. R. and Jameson, A.,Simulation of the Compressible Taylor Green Vortex using High-Order Flux Reconstruction Schemes. AIAA Paper 2014-3210, 7th AIAA Theoretical Fluid Mechanics Conference, 16-20 June 2014, Atlanta, GA.